SPRING MAGNET FILMS

J. S. Jiang, E. E. Fullerton*, C. H. Sowers, A. Inomata†, and S. D. Bader
Materials Science Division, Argonne National Laboratory, Argonne, IL 60439, USA

A. J. Shapiro and R. D. Shull
National Institute of Standards and Technology, Gaithersburg, MD 20899, USA

V.S. Gornakov and V. I. Nikitenko
Institute of Solid State Physics, Russian Academy of Sciences, 142432, Chernogolovka, Russia

Abstract—**The properties of exchange-spring-coupled bilayer and superlattice films are highlighted for Sm-Co hard magnet and Fe or Co soft magnet layers. The hexagonal Sm-Co is grown via magnetron sputtering in *a*- and *b*-axis epitaxial orientations. In both cases the *c*-axis, in the film plane, is the easy axis of magnetization. Trends in coercivity with film thickness are established and related to the respective microstructures of the two orientations. The magnetization reversal process for the bilayers is examined by magnetometry and magneto-optical imaging, as well as by simulations that utilize a one-dimensional model to provide the spin configuration for each atomic layer. The Fe magnetization is pinned to that of the Sm-Co at the interface, and reversal proceeds via a progressive twisting of the Fe magnetization. The Fe demagnetization curves are reversible as expected for a spring magnet. Comparison of experiment and simulations indicates that the spring magnet behavior can be understood from the intrinsic properties of the hard and soft layers. Estimated are made of the ultimate gain in performance that can potentially be realized in this system.**

Index Terms— **permanent magnet, exchange spring, magnetic reversal, epitaxy, sputter, thin film, superlattice, SmCo.**

I. INTRODUCTION

Understanding magnetization reversal is a fundamental issue in coupled magnetic systems. In particular, the characterization of such processes is challenging in the new class of permanent magnets known as *exchange-spring magnets* [1]. Exchange-spring magnets, or *spring magnets* for short, consist of nanodispersed hard and soft magnetic phases that are coupled at the interfaces. Such systems have the potential to achieve dramatically improved energy products because the soft majority phase significantly boosts the magnetization of the composite [2]-[4]. Since the stability of the soft phase against magnetization reversal determines the maximum achievable energy product, identifying the factors that affect the reversal process is necessary in order to realize the full potential of the exchange hardening principle.

Future applications of spring magnets will likely be based on nano-dispersed composites obtained via bulk processing [5], such as by rapid-quenching and subsequent annealing, or by mechanical alloying, to form composites with randomly oriented hard grains [6]-[8]. The measured energy products of the random nanocomposite magnets are improved over isotropic, single-phase permanent magnets, but microstructural complexities often make understanding and optimizing the properties difficult. Thin-film growth techniques, however, permit the preparation of artificial magnetic structures with nanometer-scale control of the microstructure, crystallographic orientation and magnetic anisotropy. A spring-magnet structure can be realized in thin films by interleaving hard and soft magnetic layers. Because the layered structure results in variations in the magnetic properties predominantly along the growth direction, such spring magnet films can be modeled as one-dimensional (1D) structures. Thus, coupled hard/soft magnetic multilayers retain the essential aspects of spring magnets but without the structural complexities of random nanocomposites.

We highlight herein our investigations of the exchange-spring behavior in coupled hard/soft magnetic bilayers of Sm-Co/Fe and superlattices of Sm-Co/Co grown epitaxially via sputtering in hexagonal *a*-axis and *b*-axis Sm-Co orientations. The *a*-axis films are twinned, but the *b*-axis epitaxy yields a uniaxial magnetic anisotropy. The magnetization reversal process is examined experimentally by magnetometry and magneto-optical (MO) imaging, and is compared with simulations using a 1D atomic model to provide the spin configuration for each atomic layer. Simulations for bilayers with different layer thicknesses are then used to demonstrate the optimization of the maximum energy product based on the exchange hardening principle.

II. EPITAXIAL Sm-Co HARD MAGNET FILMS

Epitaxial Sm-Co films were grown by magnetron sputtering onto Cr-buffered MgO substrates. The 200-Å Cr buffer layers are deposited onto single-crystal MgO(100) and (110) substrates at a substrate temperature of 600°C resulting in Cr(100) and (211) epitaxial growth, respectively. The Sm-Co films are subsequently deposited with a nominal Sm_2Co_7 composition by co-sputtering from separate elemental Sm and Co sources [9]. The Cr buffer layer provides strain relief from the lattice mismatch between the Sm-Co film and the MgO substrate, and also serves as a chemical barrier to interdiffusion. The buffer layer approach is of general applicability in thin-film synthesis where selectivity in phase and composition is desired [10].

DISCLAIMER

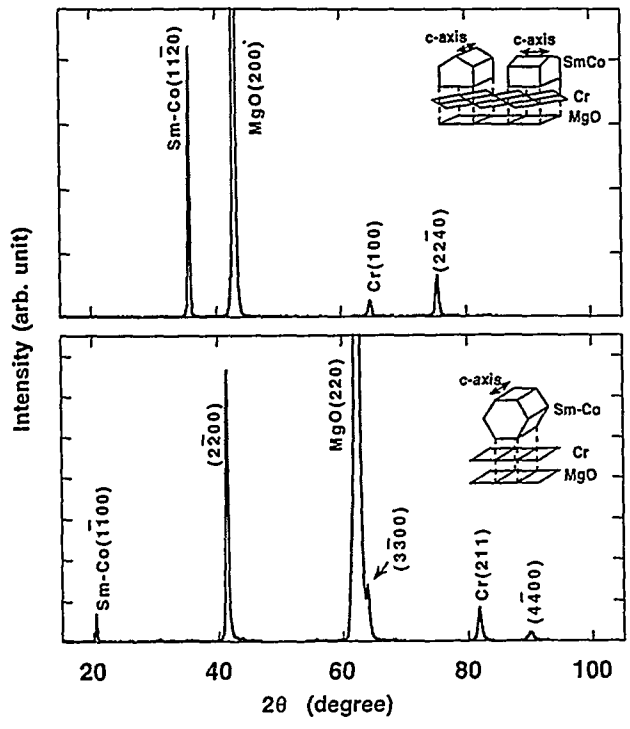

Fig. 1. X-ray diffraction patterns of Sm-Co grown epitaxially via sputtering onto Cr-coated single-crystal MgO substrates. The insets illustrate the epitaxial relations: the (11$\bar{2}$0)-oriented Sm-Co has a twinned bi-crystal structure, and the (1$\bar{1}$00)-oriented Sm-Co is uniaxial. The Sm-Co *c*-axis, which is the magnetic easy axis, lies in-plane.

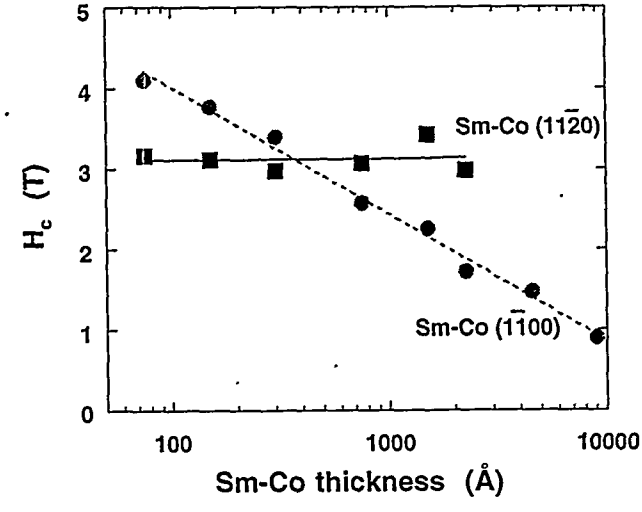

Fig. 2. The coercivity of *a*-axis and *b*-axis Sm-Co films as a function of thickness.

Shown in Fig. 1 are x-ray diffraction data for 1500-Å thick Sm-Co films deposited simultaneously onto Cr(100) and (211) buffer layers. For each buffer layer, a single orientation of the Sm-Co film is stabilized. The diffraction patterns are consistent with *a*-axis (11$\bar{2}$0) and *b*-axis (1$\bar{1}$00) Sm-Co growth onto Cr(100) and (211), respectively. These orientations are the same as those observed for Co films on Cr(100) and (211) buffers [11]. The insets illustrate the epitaxial relations. In both cases, the Sm-Co *c*-axis, the easy axis, lies in plane. The *a*-axis Sm-Co films grown onto the Cr(100) buffer are twinned, since there are two orthogonal ways to place the *hcp* Sm-Co unit cell onto the Cr(100) template. The two epitaxial relations are Sm-Co[0001] ||Cr[011]||MgO[010] and Sm-Co[0001]||Cr[01$\bar{1}$]||MgO[001]. The epitaxial relation for the *b*-axis Sm-Co films on Cr(211) is Sm-Co[0001]||Cr[01$\bar{1}$]||MgO[001].

For both orientations large coercivity values H_C are observed; the H_C values increase on cooling and are as high as 7 T at 4.2 K. The *a*-axis Sm-Co films have an effective four-fold in-plane anisotropy due to the twinning, whereas the *b*-axis Sm-Co is uniaxial with an estimated anisotropy field of ~20-25 T, comparable to those reported for bulk $SmCo_5$ (25-44 T) [12]. H_C at room temperature as a function of thickness is shown in Fig. 2 for both orientations. The distinct thickness dependences of H_C have their origins in the microstructures. A high-resolution transmission electron microscopy study [13] shows that films of both orientations consist of a mixture of $SmCo_3$, Sm_2Co_7 and $SmCo_5$ polytypoids. The resulting stacking disorder and concomitant variation in local anisotropy constants might give rise to the large H_C values. The *a*-axis Sm-Co films have orthogonally oriented crystallites seperated by a high density of twin boundaries. The formation of twin boundaries is controlled by the Sm-Co nucleation and is rather insensitive to film thickness, giving rise to a constant value of H_C for the *a*-axis films. For the *b*-axis films, H_C varies logarithmically with thickness, which points toward changes in the microstructure with increasing thickness. Atomic force microscopy shows that initial film growth is via islanding [9]. As the films thicken, the islands coalesce and the average grain size increases, which reduces H_c.

III. Sm-Co/Co SUPERLATTICES

Sm-Co/Co superlattices are prepared by depositing Sm-

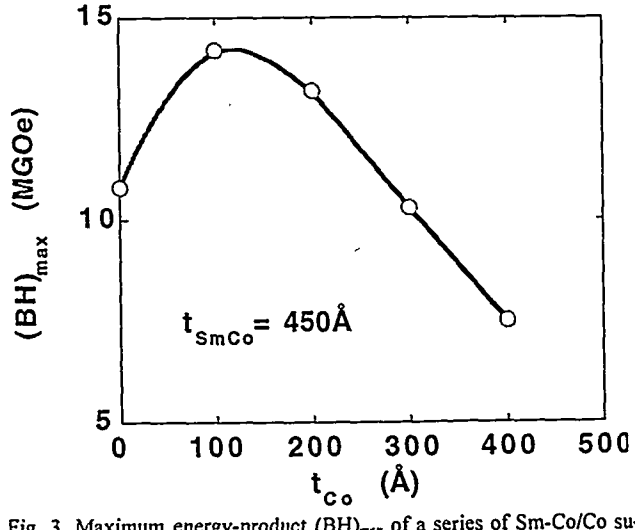

Fig. 3. Maximum energy-product $(BH)_{max}$ of a series of Sm-Co/Co superlattices as a function of Co layer thickness. The curve is a guide to the eye.

Co and Co layers onto MgO(100) substrates [14] Bright-field TEM images show the layered structure with well-defined boundaries between the Sm-Co and Co layers [14]. The superlattices are structurally coherent as evidenced by the TEM observation that in some regions the twin boundaries extends through several layers. Since the Sm-Co/Co superlattices are structurally coherent, all the Sm-Co and Co layers must have the same easy-axis direction. In this sense, the ideal structure of an aligned exchange-spring magnet is achieved in the superlattice films.

Shown in Fig. 3 is the room-temperature maximum energy product $(BH)_{max}$ extracted from the measured hysteresis loops for a series of Sm-Co/Co superlattices with fixed Sm-Co layer thickness plotted as a function of the Co layer thickness. Although a single Sm-Co layer can have a coercivity as large as 3 T, the low saturation magnetization of Sm_2Co_7 leads to a modest $(BH)_{max}$ value of 11 MGOe. When interleaved with Co layers, the total saturation magnetization of the multilayer initially increases, $(BH)_{max}$ increases by as much as 30% to ~ 14 MGOe. Although the value of $(BH)_{max}$ is relatively low, the large percentage change in $(BH)_{max}$ clearly reflects the benefit of the exchange-spring principle. Upon further increase of the Co layer thickness, the H_c value of the superlattices decreases. Even though the total saturation magnetization continues to increase, the softening of the magnetic properties degrades $(BH)_{max}$. Thus, to realize the full potential of the exchange-spring magnets, one needs to understand the magnetization reversal process and identify factors which affect the demagnetization.

IV. Sm-Co/Fe BILAYER STRUCTURES

The simplest structure that embodies the exchange-spring principle is a Sm-Co/Fe bilayer in which the soft and hard magnetic layers are exchange coupled at the interface [15],[16]. Shown in Fig. 4 are magnetic hysteresis loops for a single *b*-axis Sm-Co film and Sm-Co/Fe bilayers with 25 Å and 200 Å of Fe. The hysteresis loops are measured with the field H applied along the easy axis, which is along the MgO [001]. For the Sm-Co single layer, a square loop is observed with H_C = 3.4 T. The Sm-Co saturation magnetization is ~500-600 emu/cm^3. For the bilayer with a 25-Å Fe layer, the loop shape is similar to that of a single Sm-Co layer. A square easy-axis loop is measured, indicating that the entire Fe layer is strongly coupled to the underlying Sm-Co film and that the two layers switch as a unit. Compared to the single Sm-Co film, the H_c of the bilayer is reduced by ~50% to 1.7 T. For the bilayer with 200 Å of Fe, the loop changes shape quite significantly and exhibits separate switching transitions for the Fe and Sm-Co layers. The switching field for the Sm-Co layer (0.6 - 0.7 T) is only 20% of that of a single Sm-Co film.

The magnetization reversal process in a bilayer with an *a*-axis Sm-Co layer and a 500 Å Fe layer has been imaged using the magneto-optic indicator film (MOIF) technique [17]. In this technique the sample is covered by an MO film whose perpendicular response can be monitored via its Faraday effect. Since the sample magnetization is in-plane, not perpendicular, a hole is bored through the sample and the

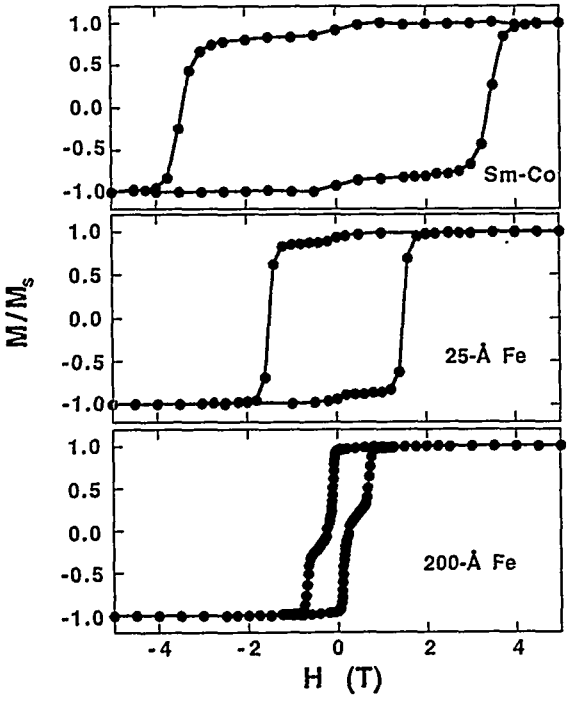

Fig. 4. Room-temperature hysteresis loops of a single Sm-Co film and Sm-Co/Fe bilayers with different Fe layer thickness.

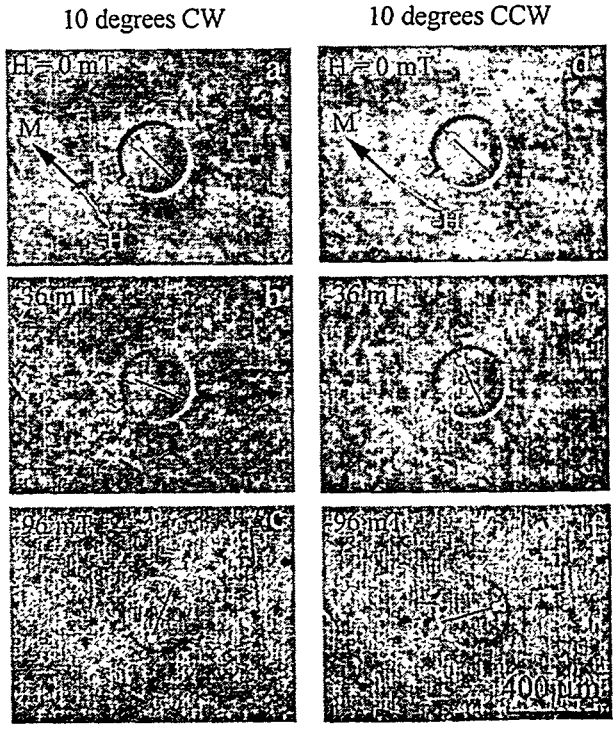

Fig. 5. MOIF images of a Sm-Co/Fe bilayer at different reverse fields. The field is applied at angle $\varphi = \pm 10°$ away from the magnetization direction of the Sm-Co hard layer.

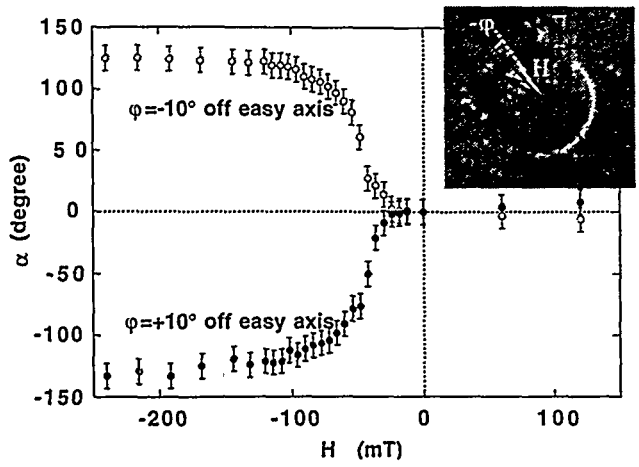

Fig. 6. Magnetization rotation angle α as a function of the reverse field H.

leakage fields around the edges are monitored. The contrast appears as *white and black* crescents due to leakage *in and out* of the film plane. The magnetization direction connects the centers of the crescents and is indicated by a schematic compass needle pointer in each image shown in Figs. 5 and 6. For the sample imaged, the magnetization behavior of the Fe layer dominates the MO contrast because the magnetic moment of the Fe layer far exceeds that in the SmCo layer.

The two sets of MOIF images in Fig. 5 show the remagnetization process of the Fe layer. The sample was initially magnetized in a 7-T field along a SmCo easy magnetization direction. A reverse field of increasing magnitude was then applied at a small angle φ=10° clockwise (CW) (Fig.5a-c) and counterclockwise (CCW) (Fig.5d-f) from the initial saturation direction. The images demonstrate there is a change in both the magnetization (M) direction and intensity as the field is reversed. Fig. 6 shows the angle α between M and the unidirectional axis as a function of H. One can see that the magnetization reversal occurs by magnetization rotation toward the field direction. It is also important to note that the rotation starts not from zero field but from a critical value H_{ex} known as the exchange field. For $H<H_{ex}$, the spins in the Fe layer couple rigidly with those of the hard SmCo layer. For

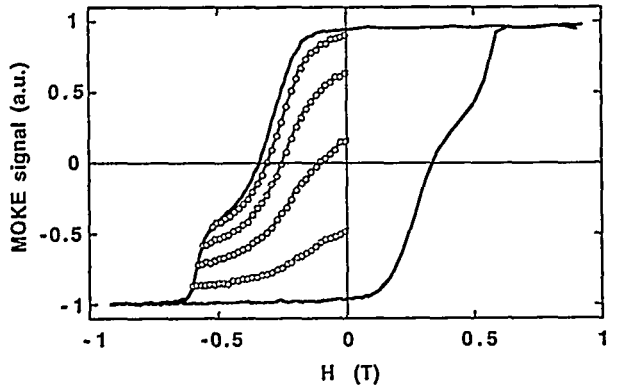

Fig. 7. Magnetic hysteresis loop and recoil curves of a Sm-Co/Fe bilayer.

$H>H_{ex}$, the spins in the Fe layer rotate toward the applied field, with the angle of rotation being zero at the interface, due to pinning by the hard layer, and increasing with distance from the interface. This non-uniform rotation in the thickness direction accounts for the reduction in MO contrast with increasing field: the leakage field from spins at different thicknesses cancels out as the twist develops.

The exchange spring behavior of the Sm-Co/Fe bilayer films is further demonstrated by measuring the irreversible magnetization change as a function of the reversal field using the magneto-optic Kerr effect (MOKE). Due to the finite penetration depth of light, the MOKE signal is dominated by the switching of the top layer which is Fe. Shown in Fig. 7 are the full hysteresis loop and recoil curves for a bilayer film with 100 Å of Fe. The Fe starts to switch at the H_{ex} = 0.22 T. For $H > H_{ex}$, a sharp drop in M is followed by an asymptotic approach to saturation until the hard layer switches irreversibly. The recoil curves are measured as follows: saturate the film, apply a reverse field of a certain magnitude, gradually decrease the field to zero while monitoring the MOKE response. It is clear from Fig. 6 that the Fe magnetization is fully reversible up to the reversal field where the Sm-Co layer switches. This winding and unwinding of the Fe layer spins are analogous to the elastic motion of a mechanical spring.

V. Numerical Simulation

We use a 1D atomic model to describe the spin configurations during magnetic reversal. The bilayer becomes a chain of spins normal to the layers, with each spin representing the moment of an atomic layer (see Fig. 8a) [18],[19]. The total energy of the system is given by:

$$E = -\sum_{i=1}^{N-1} \frac{A_{i,i+1}}{d^2}\cos(\theta_i - \theta_{i+1}) - \sum_{i=1}^{N} K_i \cos^2(\theta_i) - \sum_{i=1}^{N} HM_i \cos(\theta_i - \theta_H), \quad (1)$$

where the rotation angle for the i-th layer θ_i is measured relative to the easy direction of the hard layer, θ_H is the angle between H and the easy axis, and A_i, K_i, M_i, and d are the exchange constants, uniaxial anisotropy constants, magnetic moments and interplanar distance (set at 2 Å), respectively. The equilibrium spin configuration for a given value of H is determined by minimizing Eq. (1) using an iterative approach outlined by Camley [20], as described elsewhere [16].

Shown in Fig. 8b is the comparison of the calculated Sm-Co/Fe(200 Å) demagnetization curves to the ones measured at 25 K. Included are both the longitudinal and transverse M with respect to H. The parameters used in the calculation are, for the hard layer, A_h=1.2x10^{-6} ergs/cm, K_h=5x10^7 ergs/cm^3, M_h = 550 emu/cm^3; for the soft layer, A_s=2.8x10^{-6} ergs/cm, K_s=10^3 ergs/cm^3, M_s = 1700 emu/cm^3, the interface exchange constant A_{int} = 1.8x10^{-6} ergs/cm, and

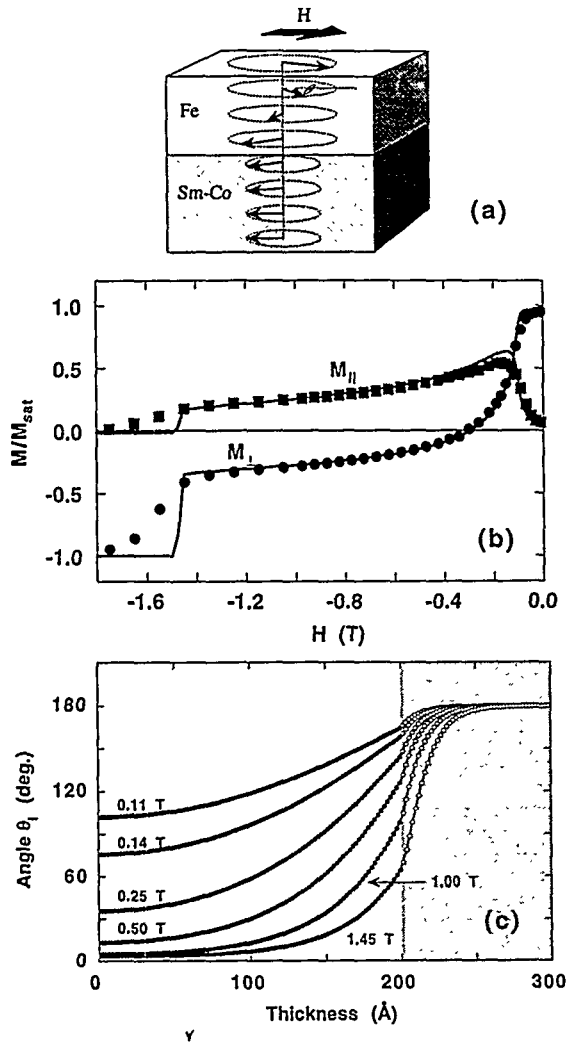

Fig. 8. (a) Schematic illustration of the 1D atomic model used in the simulation. (b) Demagnetization curves (longitudinal component $M_{\parallel}$, and transverse component $M_{\perp}$) of a Sm-Co/Fe(200 Å) bilayer structure. The solid curves are results of numerical calculations using the intrinsic parameters of the individual layers. (c) Calculated equilibrium spin configuration of a Sm-Co/Fe(200 Å) bilayer structure at several reversal fields.

θ_H=3°. The values of K_h and M_h were estimated from magnetization measurements on the Sm-Co films. The calculation reproduces the H_{ex} value, the field dependence of both the longitudinal and transverse magnetization, as well as the switching field of the Sm-Co layer at ≈1.5 T. The value of A_{int}, which is intermediate between the exchange coupling of the hard and soft layers, reflects the strong interfacial coupling. With a large interfacial exchange energy, the moments in the soft layer near the interface are pinned by the hard layer. Shown in Fig. 8c is the spin configuration at several reverse fields for the calculated M in Fig. 8b As expected, the distribution of moments is consistent with the expectation that the Fe located away from the interface rotates more. As H increases, the interfacial Sm-Co spin is also increasingly rotated and a domain wall is slowly introduced into the hard

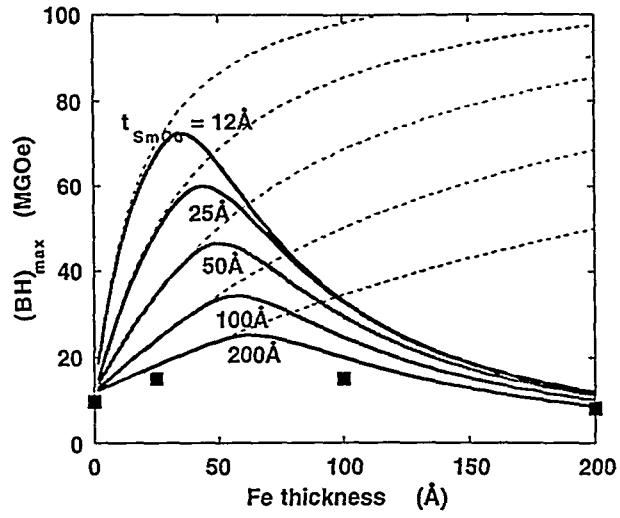

Fig. 9. Calculated maximum energy product $(BH)_{max}$ of Sm-Co/Fe bilayers with different layer thickness. The dashed curves are for the ideal $(BH)_{max}=(2\pi M)^2$. The theoretical $(BH)_{max}$ of Nd-Fe-B is 64 MGOe and typical values for commercial material are <50 MGOe.

layer. At a field such that the domain wall energy density in the soft layer becomes greater than that in the hard layer, the domain wall in the soft layer moves into, and switches, the hard layer [1].

With these parameters we can simulate a series of hysteresis loops for bilayers with different Fe and Sm-Co thicknesses and extract the maximum energy product $(BH)_{max}$. Calculated $(BH)_{max}$ curves are shown in Fig. 9. Also shown (dashed curves) is the ideal $(BH)_{max} = (2\pi M)^2$, where M is the total saturation magnetization [21]. For thin Fe (less than the Bloch wall width in the hard layer), the Fe layer couples rigidly to the hard layer and $H_{ex} > 2\pi M$. $(BH)_{max}$ then increases as a result of the increased M, following the ideal curve. With increasing thickness, the Fe-layer magnetization reverses at lower fields, and $(BH)_{max}$ is limited by H_{ex}. The square symbols represent the $(BH)_{max}$ values taken from measured hysteresis loops for the bilayers. The calculation agrees with the experimental data and also resembles the $(BH)_{max}$ curve for Sm-Co/Co superlattices in Fig. 3. The calculations show that for thin bilayers, $(BH)_{max}$ can potentially even be greater than that for Nd-Fe-B, illustrating the importance of the exchange hardening mechanism. The calculations, however, assume that bulk constants can describe even nm-thick layers, but further experiments will be needed to see to what extent this assumption is justified.

VI. Conclusions

The magnetization reversal process in exchange spring magnets is examined experimentally in thin-film Sm-Co/Fe bilayer and Sm-Co/Co superlattice structures. The results are compared with numerical solutions of a 1D atomic model, to indicate that exchange-spring behavior can be understood from the intrinsic properties of the hard and soft magnetic phases. Besides revealing the fundamental aspects of the

magnetization reversal in spring magnets, our system addresses the microstructural influences on the hard magnetic properties. It also realistically estimates the ultimate performance achievable in permanent magnets based on the exchange-hardening mechanism, and serves as a guideline for the development of more complex nanostructures with optimized properties.

ACKNOWLEDGMENT

The work at Argonne was supported by the U. S. Department of Energy, Basic Energy Sciences-Material Sciences under contract No. W-31-109-ENG-38.

REFERENCES

* Present address: IBM Almaden Research Center, San Jose, CA 95120
† Permanent address: Fujitsu Ltd., Atsugi, Japan.

[1] E. F. Kneller and R. Hawig, "The exchange-spring magnet: A new material principle for permanent magnets", IEEE Trans. Mag., vol. 27, pp. 3588-3600, (1991).
[2] J. M. D. Coey and R. Skomski, "New Magnets from interstitial intermetallics", Physica Scripta, vol. T49, pp. 315-321, (1993).
[3] R. Skomski and J. M. D. Coey, "Giant energy product in nanostructured two-phase magnets", Phys. Rev., vol. B48, pp. 15812-15816, (1993).
[4] R. Fischer, T. Leinewebber, and H. Kronmüller, "Fundamental magnetization processes in nanoscaled composite permanent magnets", Phys. Rev., vol. B57, pp. 10723-10732, (1998).
[5] J. M. D. Coey, "Permanent Magnetism", Solid State Commun., vol. 102, pp. 101-105 (1997).
[6] J. Ding, P. G. McCormick, and R. Street, "Remanence enhancement in mechanically alloyed isotropic Sm_7Fe_{93}-nitride", J. Magn. Magn. Mater., vol. 124, pp. L1-4, (1993).
[7] L. Withanawasam, G. C. Hadjipanayis, and R. F. Krause, "Enhancedremanence in isotropic Fe-rich melt-spun Nd-Fe-B ribbons", J. Appl. Phys., vol. 75, pp. 6646-6648 (1994).
[8] R. Coehoorn, D. B. de Mooij, and C. De Waard, "Meltspun permanent magnet materials containing Fe_3B as the main phase", J. Magn. Magn. Mater., vol. 80, pp. 101-104, (1989).
[9] E. E. Fullerton, J. S. Jiang, C. Rehm, C. H. Sowers, S. D. Bader, J. B. Patel, and X. Z. Wu, "High Coercivity, Epitaxial Sm-Co Films with Uniaxial Anisotropy", Appl. Phys. Lett., vol. 71, pp. 1579-1581, (1997).
[10] E. E. Fullerton, C. H. Sowers, J. E. Pearson, S. D. Bader, X. Z. Wu, and D. Lederman, "A General Approach to the Epitaxial Growth of Rare-Earth-Transition-Metal Films", Appl. Phys. Lett., vol. 69, pp. 2438-2440 (1996).
[11] A. Nakamura, M. Koguchi, and M. Futamoto, "Microstructure of Co/Cr bilayer films epitaxially grown on MgO single-crystal substrates", Jpn. J. Appl. Phys., vol. 34, pp. 2307-2311, (1995).
[12] K. J. Strnat and R. M. W. Strnat, "Rare earth-cobalt permanent magnets"J. Magn. Magn. Mater., vol. 100, pp. 38-56. (1991).
[13] M. Benaissa, K. Krishnan, E. E. Fullerton and J. S. Jiang, "Magnetic anisotropy and its microstructural origin in epitaxially grown SmCo thin films", IEEE Trans. Mag., vol. 34, pp. 1204-1206, (1998).
[14] E. E. Fullerton, J. S. Jiang, C. H. Sowers, J. E. Pearson, and S. D. Bader, "Structure and magnetic properties of exchange-spring Sm-CO/Co superlattices", Appl. Phys. Lett., vol. 72, pp. 380-382, (1998).
[15] J. S. Jiang, E. E. Fullerton, M. Grimsditch, C. H. Sowers, and S. D. Bader, "Exchange-Spring Behavior in Epitaxial Hard/Soft Magnetic Bilayer Films", J. Appl. Phys., vol. 83, pp. 6238-6240, (1998).
[16] E. E. Fullerton, J. S. Jiang, M. Grimsditch, C. H. Sowers, and S. D. Bader, "Exchange-Spring Behavior in Epitaxial Hard/Soft Magnetic Bilayers", Phys. Rev., vol. B58, pp. 12193-12200, (1998).
[17] L. H. Bennett, R. D. McMichael, L. J. Swartzendruber, S. Hua, D. S. Lashmore, A. J. Shapiro, V. S. Gornakov, L. M. Dedukh, V. I. Nikitenko, "Magneto-optical indicator film observation of domain structure in magnetic multilayers", Appl. Phys. Lett., vol. 66, pp. 888-890, (1995).
[18] K. Mibu, T Nagahama and T. Shinjo, "Reversible magnetization process and magnetoresistance of soft-magnetic (NiFe)/hard-magnetic (CoSm) bilayers", J. Magn. Magn. Mater., vol. 163, pp. 75-79, (1996).
[19] S. Wüchner, J. C. Toussaint and J. Voiron, "Magnetic properties of exchange-coupled trilayers of amorphous rare-earth-cobalt alloys", Phys. Rev., vol. B55, pp. 11576-11585, (1997).
[20] R. E. Camley, "Surface spin reorientation in thin Gd films on Fe in an applied magnetic field", Phys. Rev., vol. B35, pp. 3608-3611, (1987).
[21] K. H. J. Buschow, "New developments in hard magnetic materials", Rep. Prog. Phys., vol. 54, pp. 1123-1213, (1991).